ICSV 17
THE 17th INTERNATIONAL CONGRESS ON SOUND & VIBRATION
CAIRO 18 - 22 JULY, 2010

SEISMIC RESPONSE CONTROL OF A BUILDING USING MR DAMPER WITH OPTIMAL STATIC OUTPUT FEEDBACK

Sharadkumar Purohit and Naresh K. Chandiramani

Department of Civil Engineering, Indian Institute of Technology Bombay, Powai 400076 Mumbai, India
e-mail: p7purohit@civil.iitb.ac.in

Control of seismic response of a ten storey building fitted with magnetorheological (MR) damper is considered. Control force desired from the MR damper is obtained using Optimal Static Output Feedback (OSOF) control. Damper dynamics is modeled using modified Bouc-Wen element. This exhibits a non-linear relationship between damper force and input-voltage/states, making it difficult to obtain the input voltage required to realize a desired control force. Hence, two control voltage laws based on the MR constraint filter, i.e., Inverse Quadratic Voltage Law (IQVL) and Inverse On-Off Voltage Law (IOOVL), are proposed as an alternative to exactly predicting the force-voltage inverse dynamics. Maximum values of peak and RMS response quantities (Interstorey Drift, Displacement, Acceleration) are obtained for controlled building response using OSOF control with IQVL, IOOVL and an existing Clipped Voltage Law (CVL). These are compared with Linear Quadratic Guassion (LQG) control using the three voltage laws and with passive-on control using constant (saturation) voltage. A reduction in maximum peak and RMS values of interstorey drift and displacement is obtained when using OSOF control as compared to passive-on/LQG control. This is not uniformly true for maximum peak accelerations vis-a-vis passive-on control. Parametric studies regarding sensor configuration (i.e., type of output measured, placement and number of sensors), state weighting matrix $\mathbf{Q}$ (pertaining to displacement-, interstorey drift-, acceleration- based performance index), and control input weighting matrix $\mathbf{R}$, are performed in order to obtain the most effective controller.

1. Introduction

Semi-active devices hold promise for vibration control since their properties can be adjusted in real time. The MR damper is a semi-active device that uses MR fluids exhibiting controllable yield characteristics and produces sizeable damping force for small input voltage.

Various parametric models have been developed to describe the behavior of MR dampers. These are based on mechanical elements, i.e., friction, spring, damper, and hysterisis elements. A Bingham

model was proposed by Stanway et al. [1], yielding good force-displacement behavior but poor force-velocity response, due to the inability of the piecewise linear model to capture hysteretic behavior. The hysteretic force was modeled via an evolutionary variable and loop control parameters by Wen [2], giving rise to the class of Bouc-Wen models for MR dampers. Wong et al. [3] studied the influence of loop control parameters and obtained a wide variety of hysteresis loops, thus establishing the Bouc-Wen models versatility in matching experimental data, except near small velocities. This shortcoming was rectified by Spencer et al. [4] in their modified Bouc-Wen model. Therein, additional damping and stiffness elements were used to model the behavior at low velocities and the accumulator, respectively. The voltage dependent model parameters were determined using test data for periodic/random displacement input and constant/random voltage input.

Various methods for controller design have been used with MR damper. Dyke et al. [5] implemented acceleration feedback based LQG control for a three storey building with modified Bouc-Wen model for the MR damper. The desired damper force was obtained using measured output consists of acceleration, displacement and damper force. Input voltage for MR damper was obtained via Clipped Voltage Law (CVL). Jansen and Dyke [6] compared various control strategies, i.e., Lyapunov control, Decentralized bang-bang control, Modulated homogeneous friction control and LQG control with acceleration feedback, using different voltage laws for each of these strategies. Chang and Zhou [7] used LQR control and modified Bouc-Wen MR damper model for a seismically excited three storey building. The inverse dynamics of the damper was modeled with a recurrent neural network using a MR constraint filter, so as to obtain the required voltage for given damper force.

In this paper, OSOF control is implemented for seismic response attenuation of a ten storey building with single MR damper. The modified Bouc-Wen MR damper model is used. Two control voltage laws (IQVL, IOOVL) are proposed and implemented along with the existing CVL [5] so as to obtain the command voltage for a desired damper force. LQG control with these three voltage laws and passive-on control with constant voltage are implemented for performance comparison with OSOF control. Parametric studies are done to obtain the influence of sensor configuration (i.e., type of output being fedback, placement and number of sensors) and performance index (PI) (involving weighting of various response quantities via state weighting $\mathbf{Q}$ and varying the control weighting $\mathbf{R}$).

2. System Model

2.1 MR Damper

The force f, as given by the modified Bouc-Wen model [4], is

$$f = c_1\dot{y} + k_1(x - x_0) \tag{1}$$

and

$$\dot{y} = \frac{1}{(c_0 + c_1)}\{\alpha z + c_0\dot{x} + k_0(x - y)\} \tag{2}$$

where the evolutionary variable z is governed by

$$\dot{z} = -\gamma|\dot{x} - \dot{y}|z|z|^{n-1} - \beta(\dot{x} - \dot{y})|z|^n + A(\dot{x} - \dot{y}) \tag{3}$$

Here x, $\dot{x}$ and f are the damper displacement, velocity and force, respectively, k_1 is the accumulator stiffness, x_0 is the initial displacement of spring k_1 which produces the nominal damper force due to the accumulator, c_0 and c_1 is the viscous damping at large and low velocities, respectively, and the stiffness k_0 is used to emulate the stiffness at large velocities. The evolutionary variable z in Eq. (2) describes the hysteretic behavior of MR damper, while γ, β, A and n are loop control parameters [3]. The voltage dependency of model parameters is given as,

$$\alpha = \alpha(u) = \alpha_a + \alpha_b u; \quad c_1 = c_1(u) = c_{1a} + c_{1b}u; \quad c_0 = c_0(u) = c_{0a} + c_{0b}u \tag{4}$$

where u is the output of a first order filter, i.e.,

$$\dot{u} = -\eta(u - v) \tag{5}$$

Here v is the input voltage to the current driver. The model parameter values are as given in [4].

2.2 MR Constraint Filter - Proposed Control Law

Following Chang and Zhou [7], the limits of the evolutionary variable z is given as,

$$z_u = \pm \left(\frac{A}{\gamma + \beta} \right)^{\frac{1}{n}} \tag{6}$$

Using Eqs. (2) and (1) neglecting stiffness terms (being small, numerically) along with the steady state solution of Eq. (5) (i.e. $u = v$), the bounds of the MR damper force f are approximated by,

$$f \approx \frac{(c_{1_a} + c_{1_b} v)}{[(c_{0_a} + c_{1_a}) + (c_{0_b} + c_{1_b})v]} [(\alpha_a + \alpha_b v) z_u + (c_{0_a} + c_{0_b} v)\dot{x}] \tag{7}$$

Substituting the values of model parameters as given in [4] into Eq. (7), f_{min} and f_{max} produced by the damper is obtained for applied voltage $v = 0$ V and $v = 2.25$ V, respectively. The realizable force region of MR damper obtained, using positive and negative values of z_u for first and third quadrants, respectively, is shown in Fig. 1. This is termed the MR constraint filter [7].

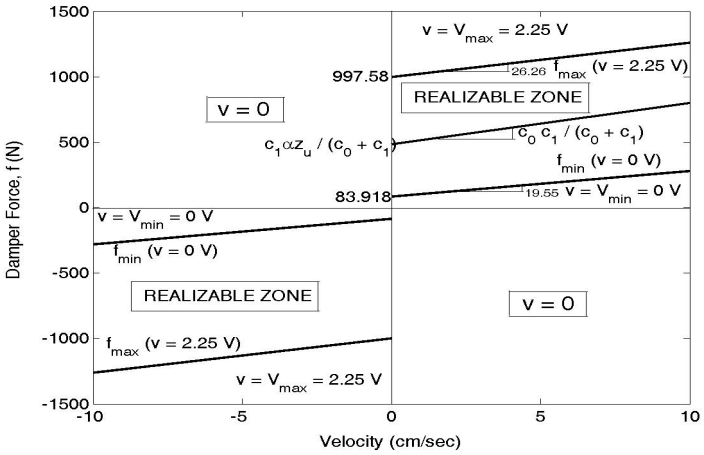

Figure 1. Realizable MR damper force zone in first and third quadrant of $f - \dot{x}$ plane.

The control laws proposed herein are based on Eq. (7) from which an inverse relation between damper force and applied voltage is obtained as,

$$\{c_{1_b}\alpha_b z_u + c_{1_b}c_{0_b}\dot{x}\}v^2 + \{(c_{1_a}\alpha_b + c_{1_b}\alpha_a)z_u + (c_{1_a}c_{0_b} + c_{1_b}c_{0_a})\dot{x} - (c_{0_b} + c_{1_b})f\}v + \{c_{1_a}\alpha_a z_u + c_{1_a}c_{0_a}\dot{x} - (c_{0_a} + c_{1_a})f\} = 0 \tag{8}$$

The required voltage for a given desired control force f_d and velocity $\dot{x}$ can be obtained via Eq. (8). The voltage predicted using z in place of z_u in Eq. (8) would be more accurate but not implementable, as z is unmeasurable. The following voltage control laws are proposed.

(1) *Inverse Quadratic Voltage Law* (IQVL): If $\dot{x} f_d > 0$ and f_d obtained lies outside the realizable region of the MR constraint filter then the control voltage is set to the appropriate limiting value, i.e., if $|f_d| > |f_{max}|$ then $v = v_{max} = 2.25$ V, else if $|f_d| < |f_{min}|$ then $v = v_{min} = 0$ V. If $\dot{x} f_d > 0$ and f_d obtained lies within the realizable region, i.e., $|f_{min}| \leq |f_d| \leq |f_{max}|$, the control voltage is obtained from Eq. (8) by substituting f_d for f, and using positive z_u if $f_d > 0$, $\dot{x} > 0$ or negative z_u if $f_d < 0$, $\dot{x} < 0$. If $\dot{x} f_d < 0$ then $v = v_{min} = 0$ V.

(2) *Inverse On-Off Voltage Law* (IOOVL): This is same as IQVL except that $v = v_{max} = 2.25$ V even when f_d lies within the realizable zone. Thus, Eq. (8) is not required in IOOVL.

2.3 Structural Model

A ten storey shear building is considered with a single damper placed at ground storey. Fig. 2 shows the structure with closed-loop feedback. Structural properties given in [8] are considered here. Nominal mass of each floor is 50 kg. Interstorey stiffnesses are 948.70, 836.99, 886.11, 889.33, 925.77, 881.83, 833.79, 824.03, 872.11 and 829.86 N/cm for first to tenth storey, respectively. Proportional (Rayleigh) damping is assumed with co-efficients $\alpha_m = 0.1$ s^{-1} and $\alpha_k = 7.36 \times 10^{-4}$ s.

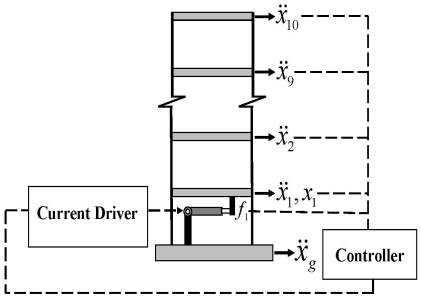

Figure 2. Ten storey building model with MR damper and closed loop feedback.

The equation of motion is given by

$$\mathbf{M}_s\,\ddot{\mathbf{x}} + \mathbf{C}_s\,\dot{\mathbf{x}} + \mathbf{K}_s\,\mathbf{x} = \mathbf{G}\,\mathbf{f} - \mathbf{M}_s\,\mathbf{L}\,\ddot{x}_g \tag{9}$$

where $\mathbf{M}_s, \mathbf{C}_s$, and $\mathbf{K}_s$ are mass, damping, and stiffness matrices, respectively as given in [8], $\mathbf{G} = [-1\ 0\ \ldots\ 0]^T$ is the location matrix of MR damper, $\mathbf{f} = [f]$ is the applied control force vector as defined by Eq. (1), $\mathbf{L} = [1\ 1\ \ldots\ 1]^T$ is the location matrix of earthquake excitation, $\ddot{x}_g$ is the earthquake excitation (ground acceleration), and $\mathbf{x} = [x_1 \quad x_2 \quad \ldots \quad x_{10}]^T$ is the displacement vector measured relative to ground. The base configuration of sensors comprises an accelerometer at each storey and an LVDT to measure drift between storeys where the MR damper is attached. Thus output vector for base configuration of sensors becomes $\mathbf{y} = [\ddot{x}_1 \quad \ddot{x}_2 \quad \ldots \quad \ddot{x}_{10} \quad x_1]^T$. Defining the state as $\mathbf{q} = [\mathbf{x} \quad \dot{\mathbf{x}}]^T$, state equations representing building dynamics (Eq. (9)) and output equations are

$$\dot{\mathbf{q}} = \mathbf{A}\,\mathbf{q} + \mathbf{B}\,\mathbf{f} + \mathbf{E}\,\ddot{x}_g\,; \qquad \mathbf{y} = \mathbf{C}\,\mathbf{q} + \mathbf{D}\,\mathbf{f} \tag{10}$$

where,

$$\mathbf{A} = \begin{bmatrix} \mathbf{0} & \mathbf{I} \\ -\mathbf{M}_s^{-1}\mathbf{K}_s & -\mathbf{M}_s^{-1}\mathbf{C}_s \end{bmatrix}; \quad \mathbf{B} = \begin{bmatrix} \mathbf{0} \\ \mathbf{M}_s^{-1}\mathbf{G} \end{bmatrix}; \quad \mathbf{E} = -\begin{bmatrix} \mathbf{0} \\ \mathbf{L} \end{bmatrix};$$

$$\mathbf{C} = \begin{bmatrix} -\mathbf{M}_s^{-1}\mathbf{K}_s & -\mathbf{M}_s^{-1}\mathbf{C}_s \\ 1\ \mathbf{0}_{1\times 9} & \mathbf{0}_{1\times 10} \end{bmatrix}; \quad \mathbf{D} = \begin{bmatrix} \mathbf{M}_s^{-1}\mathbf{G} \\ 0 \end{bmatrix}$$

MR damper dynamics is given by Eqs. (1)-(5) and model parameters as given in [4] are considered, except $x_0 = 0$ [5]. The structure is subjected to N-S component of EL Centro (1940) ground acceleration data measured at Imperial Valley.

3. OPTIMAL STATIC OUTPUT FEEDBACK CONTROL

Controller design in which desired control input (MR damper force in this case) is obtained via measured output feedback instead of state feedback, is termed LQR (Linear Quadratic Regulator) with Output Feedback [9] or Optimal Static Output Feedback Control (OSOF).

Consider structural system dynamics given by state equations and measured output equations

$$\dot{\mathbf{q}} = \mathbf{A}\,\mathbf{q} + \mathbf{B}\,\mathbf{f}_d; \qquad \mathbf{y} = \mathbf{C}\,\mathbf{q} \tag{11}$$

Here $\mathbf{f}_d$ is the desired damper force, i.e., the control input obtained by output feedback as

$$\mathbf{f}_d = -\mathbf{K}\,\mathbf{y} \tag{12}$$

where $\mathbf{K}$ is the matrix of constant feedback gains to be determined. In OSOF regulator design, $\mathbf{K}$ and hence $\mathbf{f}_d$ are determined such that the quadratic Performance Index (PI) defined as

$$J^* = \frac{1}{2}\int_0^\infty [\ \mathbf{q}^T\,\mathbf{Q}\,\mathbf{q} + \mathbf{f}_d^T\,\mathbf{R}\,\mathbf{f}_d\ ]\ \mathrm{d}t \tag{13}$$

is minimized. Here, $\mathbf{Q}$ is the positive semi-definite state weighting matrix and $\mathbf{R}$ is the positive definite control input weighting matrix.

Following Lewis and Syrmos [9], design equations to determine constant feedback gain $\mathbf{K}$ are given as,

$$\mathbf{A}_c^T\mathbf{P} + \mathbf{P}\mathbf{A}_c + \mathbf{C}^T\mathbf{K}^T\mathbf{R}\mathbf{K}\mathbf{C} + \mathbf{Q} = \mathbf{0} \tag{14}$$

$$\mathbf{A}_c\mathbf{S} + \mathbf{S}\mathbf{A}_c^T + \tilde{\mathbf{Q}} = \mathbf{0} \tag{15}$$

$$\mathbf{R}^{-1}\mathbf{B}^T\mathbf{P}\mathbf{S}\mathbf{C}^T(\mathbf{C}\mathbf{S}\mathbf{C}^T)^{-1} = \mathbf{K} \tag{16}$$

which minimizes an optimal cost (PI) expressed as,

$$E[J^*] = \frac{1}{2}\ \mathbf{q}^T(0)\mathbf{P}\mathbf{q}(0) = \frac{1}{2}\ tr(\mathbf{P}\tilde{\mathbf{Q}}) \tag{17}$$

where $\tilde{\mathbf{Q}} \equiv \mathbf{q}(0)\mathbf{q}^T(0) = \mathbf{I}$. Coupled nonlinear matrix Eqs. (14), (15), (16) can be solved using various available iterative algorithms. The algorithm of Moerder and Calise is used here [9].

4. RESULTS AND DISCUSSIONS

Response for earthquake excitation record of 10 s has been obtained at time interval $\Delta t = 0.02$ s. The following cases are considered: (1) Passive-on Control : A constant saturation voltage $v = 2.25$ V is applied to obtain the damper force. (2) Semi-active Control : Desired control force $\mathbf{f}_d$ is determined using either OSOF or LQG control method. Then voltage applied to the damper is obtained via either of the voltage laws (i.e., IQVL, IOOVL and CVL). The first-order ODE's (Eqs. (2), (3), (5)) pertaining to MR damper and the state equations pertaining to structural system dynamics (Eq. (10)) were simultaneously solved using MATLAB module ODE45 (4^{th}/5^{th} order Runge - Kutta method). Initial conditions used are comprise a null vector, as system is at rest initially.

4.1 Peak and RMS Response

State weighting $\mathbf{Q}$ used in PI (Eq. (13)) weights top storey acceleration only, i.e, $\mathbf{Q} = \mathbf{C}^T\hat{\mathbf{Q}}\mathbf{C}$, $\hat{\mathbf{Q}} = \mathrm{diag}[\mathbf{0}\ 1]$ while $\mathbf{R} = [R]$ since the control input is a scalar. The PI for passive-on control is determined using the respective $\mathbf{Q}$ and R of semi-active controllers. The OSOF controllers are compared with passive-on and LQG controllers in Table 1 for maximum peak and RMS values of Interstorey drift, displacement, and acceleration, peak and RMS damper force, and PI. The base configuration of sensors as described in Section 2.3 and denoted as (10A,1ID) is considered. The value of R indicated corresponds to the most effective control. Quantities in parentheses and square brackets correspond to percentage change (reduction shown negative) when compared and normalized with passive-on control and LQG control results, respectively.

When comparing passive-on control with uncontrolled response, the reduction in maximum peak and RMS value is $21.12\,\%$ and $28.27\,\%$, respectively, for interstorey drift, $36.55\,\%$ and $32.67\,\%$, respectively, for displacement, and $15.20\,\%$ and $20.90\,\%$, respectively, for accelerations. It is evident

from Table 1 that OSOF control achieves substantial reduction (i.e., $> 12\%$) of interstorey drift and displacement as compared to passive-on control. Corresponding maximum RMS acceleration reduces substantially, but reduction in maximum peak acceleration is marginal(e.g. 3.42%, OSOF-IQVL) except OSOF-CVL for which it is substantially higher (22.91%). Peak damper forces generated are marginally higher when using OSOF control compared to passive-on/LQG control. Corresponding RMS damper forces are considerably lower compared to passive-on control but considerably higher vis-a-vis LQG control. Lowest PI result from OSOF control as compared to passive-on/LQG control, proving the effectiveness of this control method. In comparison to passive-on control, LQG affords moderate to substantial attenuation of maximum peak and RMS values of responses with the exception of maximum peak acceleration. Peak damper forces are marginally lower while RMS damper forces are substantially lower when using LQG compared to passive-on control. LQG yields lower PI compared to passive-on control.

When comparing OSOF with LQG control, the former yields considerable reduction in maximum peak and RMS values of all responses. Thus, OSOF control is quite effective for seismic response attenuation of ten storey building with single MR damper as compared to passive-on/LQG control. The proposed control voltage laws IQVL and IOOVL perform marginally better than existing CVL when using LQG, and are comparable to CVL when using OSOF control. Storeywise and time trace, comparison among passive-on and semi-active controllers are not included here.

Table 1. Maximum peak and RMS response, passive-on, semi-active control for base configuration of sensors

Response Quantity	Uncon--trolled	Passive On	OSOF			LQG		
			CVL	IQVL	IOOVL	CVL	IQVL	IOOVL
			R=10^{-06}	R=10^{-06}	R=10^{-08}	R=10^{-06}	R=10^{-06}	R=10^{-06}
Max. RMS Interstorey Drift (cm)	1.3765	0.9873	0.7761 (-21.39) [-6.85]	0.7741 (-21.60) [-4.89]	0.7654 (-22.48) [-4.75]	0.8332 (-15.61)	0.8139 (-17.56)	0.8036 (-18.61)
Max. Peak Interstorey Drift (cm)	3.617	2.853	2.4710 (-13.39) [-11.02]	2.463 (-13.67) [-11.24]	2.4837 (-12.94) [-7.25]	2.777 (-2.66)	2.7749 (-2.74)	2.6779 (-6.14)
Max. RMS Displacement (cm)	8.893	5.9873	4.9061 (-18.06) [-8.66]	4.8745 (-18.59) [-7.11]	4.8123 (-19.62) [-6.89]	5.3713 (-10.29)	5.2475 (-12.36)	5.1681 (-13.68)
Max. Peak Displacement (cm)	23.622	14.987	12.844 (-14.30) [-14.27]	12.730 (-15.06) [-11.51]	12.618 (-15.81) [-10.16]	14.982 (-0.03)	14.385 (-4.02)	14.045 (-6.29)
Max. RMS Acceleration (cm/sec^2)	388.84	307.56	253.47 (-17.59) [-5.56]	253.56 (-17.56) [-1.46]	258.21 (-16.05) [-0.33]	268.39 (-12.74)	257.31 (-16.34)	259.07 (-15.77)
Max. Peak Acceleration (cm/sec^2)	1102	934.5	1148.6 (+22.91) [-9.82]	902.54 (-3.42) [-16.93]	915.02 (-2.08) [-22.39]	1273.7 (+36.30)	1086.5 (+16.27)	1179 (+26.14)
RMS MRD Force (N)		667.19	509.74	530.84	527.44	406.39	437.53	450.94
Peak MRD Force (N)		1269.3	1309.1	1303.6	1289.6	1256.7	1252.7	1243.3
PI Semi-active			66.84	67.11	66.7	73.69	68.12	69.15
PI Passive-on			99.04	99.04	94.64	99.04	99.04	99.04

4.2 Parametric Studies

Various other sensor configuration (considering type of output measured, numbers, placement), state weighting $\mathbf{Q}$, and control weighting $\mathbf{R}$ are now considered in order to explore the possibility of better control and/or more efficient sensor usage (i.e., numbers, placement). Table 2 shows the sensor configurations considered (10A,1ID) being base configuration of sensors considered in section 4.1.

State weighting $\mathbf{Q}$, pertaining to various alternative weightings of response quantities as considered in the PI (Eq. (13)), are, $Q_1 \rightarrow$ Top storey Acceleration ($\mathbf{C^T}\hat{\mathbf{Q}}\mathbf{C}$, $\hat{\mathbf{Q}} = diag[\mathbf{0}\ 1]$), $Q_2 \rightarrow$ Total energy of system (diag[$\mathbf{K}_s\ \mathbf{M}_s$]), $Q_3 \rightarrow$ Top storey Displacement ($\mathbf{0}$ except $\mathbf{Q}_{10,10} = 1$) and $Q_4 \rightarrow$ Lowest storey Interstorey Drift and top storey Displacement ($\mathbf{0}$ except $\mathbf{Q}_{1,1} = \mathbf{Q}_{10,10} = 1$).

Table 2. Various sensor configurations for a ten storey building

Storey No.	Sensor Configurations (○ Accelerometer × LVDT Sensor)								
	10A,1ID	5ID(1)	10ID	3A,3ID	3A,1ID	10A,10ID	10A	5A	5ID(2)
10	○		×	○	○	○ ×	○	○	×
9	○	×	×			○ ×	○		
8	○		×	○		○ ×	○	○	×
7	○	×	×		○	○ ×	○		
6	○		×	○		○ ×	○		×
5	○	×	×	×		○ ×	○		
4	○		×		○	○ ×	○		×
3	○	×	×	×		○ ×	○	○	
2	○		×			○ ×	○	○	×
1	○ ×	×	×	×	×	○ ×	○	○	

For each sensor configuration, results for the controller (comprising control method, voltage law, state weighting $\mathbf{Q}$ and R) yielding most effective control is reported in Table 3. Quantities in parentheses denote percentage change when compared and normalized with passive-on control results of Table 1. Quantities in square brackets denote percentage change when compared and normalized with the most effective complimentary controller, i.e., if the most effective controller is based on OSOF then the most effective complimentary controller is based on LQG and vice-versa. The sensor configurations and corresponding most effective complimentary controller are: (5ID(1))→(LQG-IOOVL, Q_3, $R = 10^{-19}$); (10ID)→(LQG-IQVL, Q_1, $R = 10^{-11}$); (10A,10ID)→(LQG-IQVL, Q_2, $R = 10^{-09}$); (3A,1ID)→(OSOF-IOOVL, Q_1, $R = 10^{-15}$); (3A,3ID)→(OSOF-IOOVL, Q_1, $R = 10^{-07}$); (10A)→(OSOF-IOOVL, Q_1, $R = 10^{-09}$); (5A)→(OSOF-CVL, Q_1, $R = 10^{-05}$). For sensor configuration (5ID(2)), passive-on control is most effective, and hence the most effective complimentary controller is also the most effective semiactive controller, i.e., (OSOF-IQVL, Q_3, $R = 10^{-15}$).

It is evident that semi-active controllers perform better than passive-on control for all sensor configurations except (5ID(2)). Both semi-active controllers yield substantial reduction in maximum peak/RMS values of interstorey drift and displacement, and also maximum RMS acceleration, compared to passive-on control. However, maximum peak accelerations are higher except for (3A,1ID) and (10A) sensor configurations. The PI are lower for the semi-active controllers compared to passive-on control. Comparing percentages in parentheses with those in square brackets, it can be inferred that, for (10A,10ID) and (3A,3ID) configurations the performance of the most effective controller and most effective complimentary controller are comparable, i.e., OSOF-IQVL and LQG-IQVL are comparable for (10A,10ID), and LQG-IOOVL and OSOF-IOOVL are comparable for (3A,3ID).

5. Conclusion

OSOF controllers perform well compared to passive-on/LQG controllers for base configuration of sensors case. Parametric study reveals that, when using only interstorey drift feedback, OSOF control performs better than passive-on and LQG control, with the later performing worst. OSOF control requires interstorey drift feedback along with acceleration feedback to have effective control. An effective semi-active controller can be designed using as few as four sensors. The PI contains either total system energy or top storey displacement whenever semi-active control is most effective.

Table 3. Maximum peak and RMS response of best semi-active control for various sensor configurations

Response Quantity	Sensor Configurations							
	5 ID(1)	10 ID	10A,10ID	3A,1ID	3A,3ID	10A	5A	5ID(2)
	OSOF	OSOF	OSOF	LQG	LQG	LQG	LQG	Passive
	IOOVL	IOOVL	IQVL	CVL	IOOVL	IQVL	IOOVL	On
	Q_2	Q_3	Q_2	Q_3	Q_2	Q_2	Q_2	
	R=10^{-07}	R=10^{-11}	R=10^{-06}	R=10^{-09}	R=10^{-06}	R=10^{-11}	R=10^{-09}	
Maximum RMS Interstorey Drift (cm)	0.7826 (-20.73) [-17.62]	0.7893 (-20.05) [-7.34]	0.7785 (-21.15) [-0.80]	0.7992 (-19.05) [+8.31]	0.7898 (-20.00) [-0.77]	0.7845 (-20.54) [-7.81]	0.7822 (-20.77) [-27.70]	0.9873 [+12.18]
Maximum Peak Interstorey Drift (cm)	2.4965 (-12.50) [-20.68]	2.498 (-12.44) [-17.72]	2.2494 (-21.16) [-0.47]	2.2483 (-21.20) [-18.73]	2.4052 (-15.70) [-2.50]	2.2592 (-20.81) [-24.74]	2.2873 (-19.83) [-29.93]	2.853 [-7.38]
Maximum RMS Displacement (cm)	4.9001 (-18.16) [-20.58]	4.9431 (-17.44) [-9.79]	4.8646 (-18.75) [-0.84]	4.9879 (-16.69) [+5.98]	4.9448 (-17.41) [-0.56]	4.9039 (-18.09) [-8.51]	4.8912 (-18.31) [-30.43]	5.9873 [+7.74]
Maximum Peak Displacement (cm)	12.717 (-15.15) [-32.16]	12.781 (-14.72) [-18.55]	12.750 (-14.93) [-0.65]	12.969 (-13.47) [+0.57]	12.872 (-14.11) [+0.41]	12.829 (-14.40) [-13.95]	12.796 (-14.62) [-35.93]	14.987 [-12.44]
Maximum RMS Acceleration (cm/sec^2)	268.54 (-12.69) [-15.18]	266.43 (-13.37) [-1.83]	254.20 (-17.35) [+1.89]	257.68 (-16.22) [+0.75]	262.46 (-14.66) [-1.32]	249.42 (-18.90) [-13.03]	252.02 (-18.06) [-16.90]	307.56 [-0.94]
Maximum Peak Acceleration (cm/sec^2)	1101.8 (+17.90) [-7.29]	1028.5 (+10.06) [+5.51]	992.76 (+6.23) [+9.82]	921.01 (-1.44) [-13.02]	969.48 (+3.74) [-4.27]	903.82 (-3.28) [-30.94]	950.42 (+1.70) [+1.73]	934.5 [-24.81]
PI Semi-active	560.63	0.02446	549.80	0.0280	568.31	554.07	552.21	-
PI Passive-on	819.32	0.03589	823.33	0.0403	823.33	818.88	818.88	-

REFERENCES

[1] R. Stanway, J. L. Sproston, N. G. Stevens, Nonlinear modelling of an electrorhelogical vibration damper, *Journal of Electrostatics*, 1987, 167–184.

[2] Y. K. Wen, Method for random vibration of hysteretic systems, *ASCE Journal of Engineering Mechanics Divison*, 1976, 249–263.

[3] C. W. Wong, Y. Q. Ni, J. M. Ko, Steady state oscillation of hysteretic differential model II : performance analysis, *ASCE Journal of Engineering Mechanics*, 1994, 2299–2325.

[4] B. F. Spencer Jr., S. J. Dyke, M. K. Sain, J. D. Carlson, Phenomenological model of a magnetorhelogical damper, *ASCE Journal of Engineering Mechanics*, 1996, 230–238.

[5] S. J. Dyke, B. F. Spencer Jr., M. K. Sain, J. D. Carlson, Modelling and control of magnetorhelogical dampers for seismic response reduction, *Smart Materials and structures*, 1996, 565–575.

[6] L. M. Jansen, S. J. Dyke, Semi-active control strategies for MR dampers: A comparative study, *Journal of Engineering Mechanics*, 2000, 795–803.

[7] C. C. Chang, L. Zhou, Neural network emulation of inverse dynamics for a magnetorhelogical damper, *ASCE Journal of Structural Engineering*, 2002, 231–239.

[8] K. V. Yuen, Y. Shi, J. L. Beck, H. F. Lam, Structural protection using MR dampers with clipped robust reliability-based control, *Structural Multidisciplinary Optimization*, 2007, 431–443.

[9] F. L. Lewis, V. L. Syrmos *Optimal Control*, John Wiley & Sons, Inc.:New York, USA, 1995.